## EDGE ARTICLE

Check for updates

# Effect of modulator connectivity on promoting defectivity in titanium–organic frameworks†

Isabel Abánades Lázaro, [ID] Neyvis Almora-Barrios, [ID] Sergio Tatay [ID] and Carlos Martí-Gastaldo [ID] *

The recognition of defect chemistry as a true synthetic tool for targeted creation of defects and controllable performance remains limited by the pool of frameworks explored. The value of defect engineering in controlling the properties of defective frameworks has been beautifully exemplified and largely demonstrated with UiO-type materials based on Zr(IV) nodes. However, titanium–organic frameworks remain largely unexplored in this context arguably due to the complex chemistry in solution of Ti(IV) and the difficulties in growing crystalline solids. We report a systematic study on the ability of mono- and dicarboxylic modulators (benzoic and isophthalic acid) to promote defect creation in the heterometallic Ti-MOF of the MUV-10 family. Our results indicate that both acids behave as capping modulators at high concentrations, but isophthalic acid is a more efficient defect promoter, yielding defective phases with nearly 40% of missing linkers. Our computational results suggest that this difference cannot be solely ascribed to relative changes in acidity but to the ability of this bidentate linker in compensating the structural distortion and energy penalty imposed by breaking the connectivity of the underlying framework.

## Introduction

The controlled introduction of defects in Metal–Organic Frameworks (MOFs) provides a versatile platform to modify their local structure and chemistry. This route has proven quite useful for tailoring their original properties[1–4] or endowing them with additional functions,[5,6] not easily accessible in the pristine material. The potential of defect engineering for improving and optimizing the performance of MOFs in applications such as gas storage, separation or catalysis is responsible for its increasing importance in the field.[7] As shown in Fig. 1, the total number of publications on defective frameworks has increased significantly in the last five years.

From a synthetic standpoint, the density and nature of the defects incorporated – in the form of missing linkers or nodes – can be controlled during the assembly of the framework or post-synthetically by thermal[7] and acid/base treatments.[8,9] The first approach is the most usual and relies on the use of modulators, typically monotopic ligands, that compete with the linkers for the metal coordination sites.[10] In the context of UiO-type Zr(IV)-MOFs, the addition of small amounts of monocarboxylic acids can be used to gain control over the crystallization process and enable the synthesis of large crystals with well-defined morphology,[11,12] whereas higher concentrations of these monodentate acids can be used to activate the formation of defects of variable density and nature.[13] This strategy has been used for numerous frameworks but UiO-66 remains the model material for most of these studies, and has been the focus of more than 30% of the work reported in the last five years (Fig. 1). This is possibly due to two main reasons. The chemistry of modulators was originally introduced and studied for UiO-type materials and then systematically extended to other Zr/Hf(IV) MOFs based on equivalent $Zr_6O_8/Hf_6O_8$ metal-oxo clusters, amenable to the same type of chemistry.[14] Besides, UiO-66 seems to be exceptionally prone to creating missing nodes that are structurally correlated to form the so-called reo phase.[15] These can be detected with X-ray diffraction for easier understanding of the structure-to-function relationships.

*Instituto de Ciencia Molecular (ICMol), Universidad de Valencia, Catedrático José Beltrán-2, 46980, Paterna, Spain. E-mail: carlos.marti@uv.es*

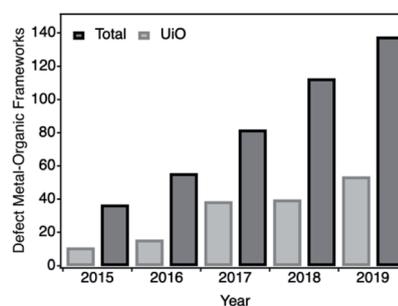† Electronic supplementary information (ESI) available. See DOI: 10.1039/d0sc06105k

**Fig. 1** Number of publications on defective metal–organic frameworks (black) and on UiO-type derivatives during the last 5 years. Data extracted from ISI Web of knowledge in August 2020.

Compared to these tetravalent metals, titanium can also be used to generate frameworks of exceptional stability and offers additional features such as its higher natural abundance, its low toxicity and its ability to endow these materials with redox and photoactive properties.[16] Though initially scarce, recent synthetic advances have expanded the pool of Ti-MOFs available that now include homo-[17–22] and heterometallic[23–25] materials with micro- and mesoporosity. However, to the best of our knowledge there are no precedents of defective titanium frameworks in the literature. Undertaking this synthetic effort is necessary to extend defect chemistry beyond UiO-type frameworks for a richer understanding of this phenomenon in order to access more diverse chemistries and topologies.

Herein, we describe a comprehensive study designed to reveal the principles that control the generation of defects in titanium frameworks by using heterometallic MUV-10(Ca)[24,25] as a model. Rather than exclusively studying the accepted effect of the modulator's acidity on defect promotion,[26] we also analyze the impact of its topicity by direct comparison of monotopic benzoic and ditopic isophthalic acids and the role of metal-linker ratios during synthesis. Our results confirm that the connectivity of the underlying framework has a direct effect on the suitability of isophthalic acid to promote defect formation in MUV-10.

## Results and discussion

### Optimization of the synthesis of defect-free MUV-10 phases

MUV-10 is built from the assembly of eight-connected $[Ti_2Ca_2(\mu_3\text{-}O)_2(H_2O)_4(CO_2)_8]$ heterometallic nodes with three-connected btc linkers (btc = benzene-1,3,5-tricarboxylate anion) to form $[Ti^{IV}Ca^{II}(\mu_3\text{-}O)(btc)_{1.33}(H_2O)_2]$, a microporous framework with a surface area of close to 1000 m$^2$ g$^{-1}$.[24] MUV-10 can be synthesised at high yields from a direct reaction of a calcium salt with different titanium sources in the presence of acetic acid as a modulator. Prior to analysing the effect of benzo and iso modulation in the promotion of defects, we studied the effect of pH modulation and crystal growth promoters on the synthesis originally reported by some of us.

We first reacted stoichiometric amounts of the metal precursors and an excess of btc (1.5 ratio) in dimethylformamide (Unmod) and in the presence of acetic acid (AcOH) or hydrochloric acid (HCl) as co-solvent modulators. For more details on the syntheses and complete characterization sets the reader is referred to ESI Sections S2 and S3,† respectively. All the samples were crystalline and phase pure, as determined by powder X-ray Diffraction (PXRD) and Fourier Transformed Infra-Red spectroscopy (FT-IR). However, AcOH modulation favours the formation of more crystalline MUV-10 phases featuring narrower and more intense diffraction lines (Fig. 2b and S1†). This effect is also extended to the size and morphology of the particles formed, as analyzed by Scanning Electron Microscopy (SEM). In contrast to AcOH, which enables the formation of octahedral crystals of 3 μm on average, HCl leads to more irregular morphologies and smaller sizes (ca. 1.5 μm), whereas nanoparticles (ca. 20 nm) are formed the case of the unmodulated sample (Fig. 2c and S3†). $^1$H-NMR analysis of the

digested samples rules out the incorporation of AcOH into the framework and reveals instead the increasing formic acid (fa) mole percent versus btc, mol% = 1, 1.5 and 3.7% for AcOH, HCl and unmodulated MUV-10, respectively. Formic acid is likely generated from the decomposition of DMF during the synthesis.[26] This correlates well with the thermogravimetric analysis (TGA, Fig. S6 and Table S5†) of the three samples that suggests the formation of almost defect-free MUV-10 in the presence of AcOH. In turn, the use of HCl and unmodulated conditions generates small degrees of defectivity, 6.4 and 10.1% of missing linkers, with slightly lower thermal stability. Compared to AcOH, N$_2$ isotherms show a minimum impact on the porosity of the MUV-10 formed with HCl whereas the unmodulated conditions promote a significant reduction in microporosity and a mesoporous tail associated with the nanosizing of the material (Fig. 2d, Table S7†).

The use of highly acidic solutions, AcOH or HCl, is required to stabilise Ti(IV) precursors in solution and prevent rapid hydrolysis and nucleation for small particle size and low crystallinity phases. Our experiments suggest that AcOH acts only as a crystal growth promoter, without getting permanently attached to the framework and minimizing defect generation. As reported for UiO-66, the p$K_a$ of the modulator controls the grafting to the metal nodes. In our case the p$K_a$ of AcOH (4.76) is approximately the same as that of btc (4.70) but less acidic than that of fa (3.70), explaining why the latter is marginally incorporated in the structure even at low concentrations. From this point on, all the syntheses were carried out with a fixed concentration of AcOH that is not included in the labels for simplification. These conditions are adequate to produce almost defect-free MUV-10 crystals, more suitable to analyze the effect of other modulators to promote defects at variable concentrations.

### Systematic exploration of the chemical space to synthesize defective MUV-10 phases

The chemistry of modulators relies on complex deprotonation and metal complexation equilibria yet to be fully understood.[11] As shown in Scheme 1, both the pH of the reaction mixture and the acidity of the modulator/organic linker are competing variables. Acid solutions will lead to a lower fraction of deprotonated species and subsequent slower nucleation and crystallization. At the same time, the use of stronger acids as modulators or linkers will yield a higher fraction of deprotonation and a stronger competition for metal complexation.

According to this complex scenario, we designed two sets of experiments (Fig. 3) that accounted, not only for the nature or concentration of the modulator, but also for the relative
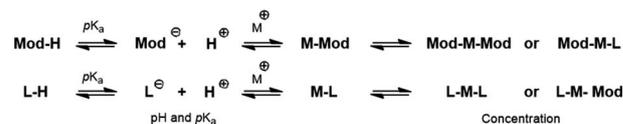
Scheme 1 Model enclosing the deprotonation and metal-complexation equilibria occurring during coordination modulation.[11]
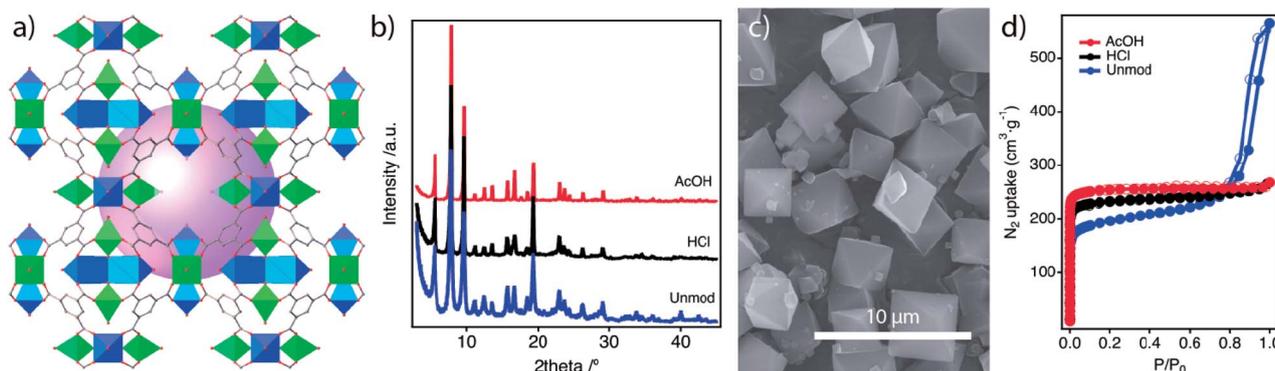
**Fig. 2** (a) Structure of MUV-10(Ca) built from heterometallic $Ti_2Ca_2$ nodes and btc linkers. Ti and Ca atoms are represented in green and blue. (b) PXRD patterns of MUV-10 samples modulated with AcOH (red) and HCl (black) or unmodulated (blue). (c) SEM picture of the octahedral crystals produced with AcOH. (d) $N_2$ isotherms at 77 K. The absence of a modulator induces the formation of more defective nanoparticles that account for the reduction in microporosity and the mesoporous tail observed at $P/P_0 > 0.8$.

concentration of the linker. The first involves the addition of increasing amounts of modulators, benzoic (benzo) or iso-phthalic acid (iso), whilst maintaining the linker to metal ratio at 1.5. This route, referred to as high btc (H), will help to analyse the effect of the modulators as the only variable in the deprotonation/complexation equilibria under the conditions more favourable for MUV-10 formation. Although this is the common approach used in the field,[26] we also decided to study the gradual replacement of the linker by the modulator starting from a btc : metal ratio of 1.[27] This route, called low btc (L), might be more effective in maximizing the effect of the modulators on incorporating defects by minimizing the impact of the linker to metal complexation. The resulting synthetic series are labelled mod%-H/L, where mod% corresponds to the modulator mole percent (mol%), the percentage of modulator per total amount of carboxylic acid (mod and btc) present in the synthesis and H or L refers to the btc : metal ratio used during the synthesis, 1.5 and <1, respectively. Additionally, we performed syntheses in which btc was totally replaced by the modulators. While in the case of benzo this did not produce any solid, the use of iso produced an independent amorphous mesoporous phase not related to MUV-10 that we denote as iso

100%. See ESI Section S2 and S4† for the detailed synthetic conditions of all sets for a total of 32 samples.

## Effect of modulator connectivity on the defect chemistry of MUV-10 phases

**Defect incorporation under conditions adequate for MUV-10 formation.** The PXRD patterns of all benzo and iso modulated samples synthesized in the H region corresponded to highly crystalline, phase pure MUV-10 phases (Fig. 4a and b). Compared to benzo, increasing concentrations of iso improve the crystallinity of the framework as denoted by the concomitant increase of the intensity of the (110) and (111) diffraction lines. This is a preliminary indicator of the suitability of dicar-boxylic acid in modulating the synthesis of MUV-10. ^{1}H-NMR analysis of acid-digested samples confirmed the presence of both modulators in the respective series that are complemented by formic acid likely partially compensating for defects. We used FT-IR to rule out the presence of modulators as free molecules occluded in the framework during the assembly. As shown in ESI Section S.5.2 and Fig. S8–S11,† the absence of carboxylate vibrations matching those of reference iso or benzo free linkers confirms their coordination with the metal cluster. The incorporation extent was calculated from the ^{1}H-NMR data. Fig. 4c shows the mol% (vs. total amount of ligands, btc and mod) of mod and fa incorporated into the structure compared to the modulator mol% added during the synthesis. Incorporation is remarkably more pronounced for iso than for benzo. The first escalates with the amount of modulator added in the synthesis up to a maximum of 45 mol%, compared to the 5 mol% of benzo incorporated. The efficient incorporation of iso can be correlated with the secondary role played by formate, which competes with the modulator only at low concentrations for minimum incorporation at higher concentrations. In turn, fa competition with benzo remains effective across all the concentration intervals explored. The differences in iso and benzo incorporation might be related to their relative changes in acidity and/or connectivity. The $pK_a$ of iso (3.46) is appreciably lower than that of benzo (4.20) supporting more efficient
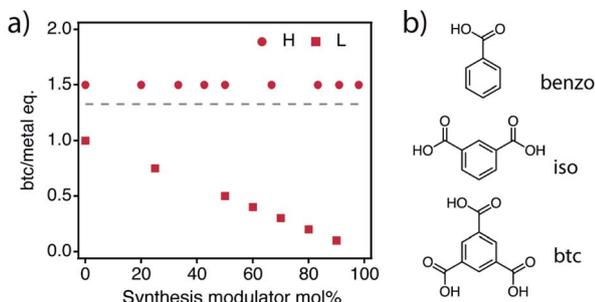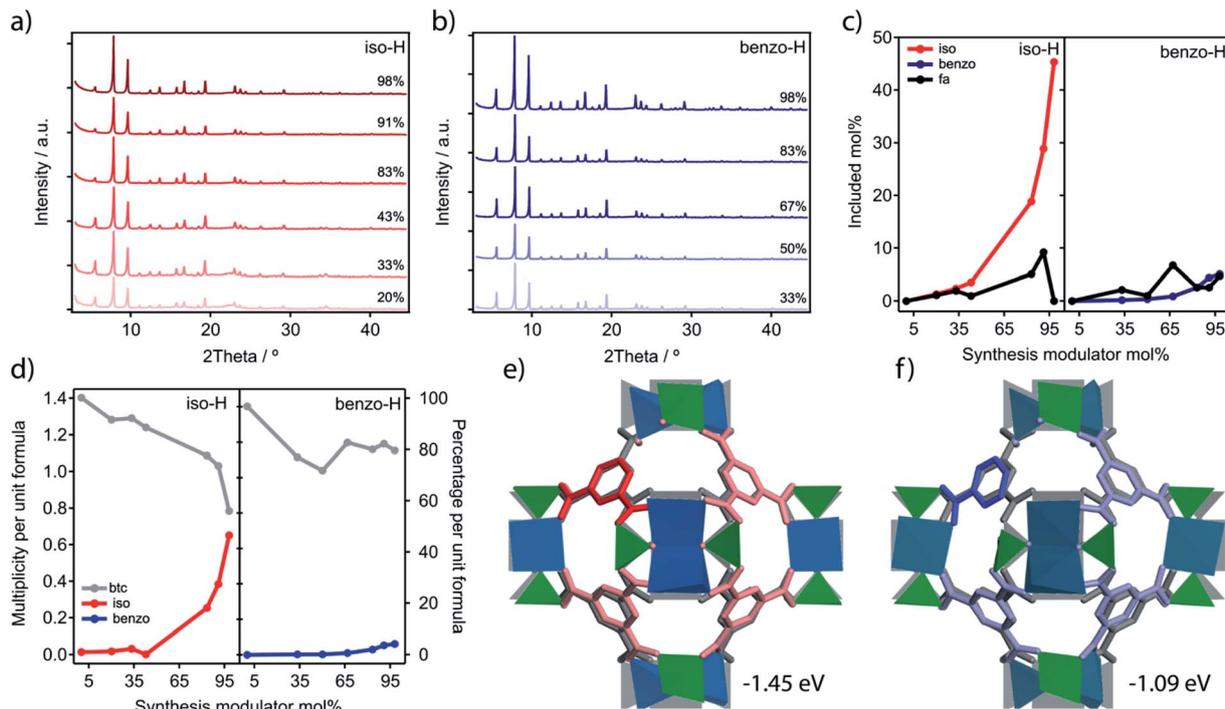


**Fig. 3** (a) Synthetic sets designed to study the impact of modulators on the promotion of defects for fixed and variable amounts of btc/metal ratios above (H) and below (L) the stoichiometric ratio fixed by the formula of MUV-10 (dashed line). (b) Modulators with increasing denticity used in this study and the linker btc.

**Fig. 4** (a) PXRD patterns of MUV-10-iso-%-H and (b) benzo-%-H series. (c) Molar fraction of the modulator and formic acid incorporated into the framework for increasing concentrations of the modulator. Experimental values determined with ^{1}H-NMR analysis. (d) Comparison of the amount of btc, isophthalic and benzoic acid in the framework in H and L regions for increasing concentrations of the modulator. Values estimated by NMR-TGA analysis of each experimental data set. DFT calculations of the enthalpy change and structural distortion to pristine MUV-10 (gray) associated with the formation of defective frameworks upon the incorporation of (e) iso (dark red) and (f) benzo (dark blue) modulators. Charge balance was compensated with $OH^-$ capping linkers in both cases.

incorporation.[26] However, the difference with fa (3.70) is quite small. This points to an additional effect of the denticity of iso, which features two connection points closer to the three in btc. This is in great agreement with reports showing that the degree of surface functionalization using hist-tags increases with the number of coordinating units.[28]

We also analyzed the chemical purity of iso-H and benzo-H samples with energy dispersive X-ray spectroscopy (EDX) and ICP analysis (ESI Section S.5.3). Both sets display Ca : Ti ratios close to ideality although we observe a slight excess of Ti with EDX, suggesting a partial enrichment of the surface of the crystals with this metal. In order to compare the linker deficiencies throughout the series, we analyzed the thermogravimetric decomposition profiles and the ^{1}H-NMR ratios using a method inspired by the seminal work of Lillerud.[26,29] We refer the reader to the methodology recently reported by one of us[30] and ESI Section S.5.4 for a detailed description of this method and the models applied for the calculation of missing linker percentages. Fig. 4d shows the evolution of btc and the modulator alongside the generation of missing linker defects per unit formula of MUV-10 for both sets of reactions. Iso-H series show a progressive decrease of btc that correlates very nicely with the incorporation of iso. Our calculations reveal a maximum close to 40% missing linkers for iso 98%-H, comparable to the 33% reported for the reo phase in defective UiO.[15,26] This trend is substantially different for benzo modulation, which shows

a much poorer efficiency in generating missing linkers, with a maximum of 14% for benzo 98%-H, because of the comparatively much smaller incorporation percentage. Besides, the defectivity in benzo does not escalate for increasing concentrations of the modulator.

Overall, our experiments confirm drastic differences between iso and benzo in their ability to promote defects, which cannot be simply ascribed to changes in their relative acidity. To understand this difference, we calculated the energy balance required for introducing missing linkers in MUV-10 ($1 \times 1 \times 1$ unit cell) compensated by iso, benzo, AcOH or fa (Fig. 4e and f and Table S23†). See ESI Section S5.5† for computational details. Our simulations show that the introduction of defects is thermodynamically possible in all cases ($\Delta E < 0$). Compared to monocarboxylic benzo and fa that display similar energy gains, the enthalpy gain for the dicarboxylic iso is −0.4 eV more favourable. Compared to monocarboxylic modulators, we argue that the efficiency of this dicarboxylic acid as a defect promoter is linked to its higher ability to compensate the energy penalty imposed by breaking the 8,3-connectivity of the underlying network.

**MUV-10 modulation under linker deficient conditions.** The ability of iso to form amorphous titanium phases in deficient concentrations of trimesic acid led us to analyse iso-L and benzo-L series separately. The phase iso 100% is not related to MUV-10 and, according to ICP, EDX, FT-IR and TGA analysis

(ESI Section S6†), agrees well with the formula $Ti(O)_{1.725}(Iso)_{0.275}$.

The PXRD patterns of iso-L (Fig. S16†) show a progressive decrease in crystallinity for increasing concentrations of the modulator for the formation of an almost amorphous solid from iso 90%-L. Moreover, ICP and EDX analysis (Table S25†) of these samples revealed an increasing deviation from unity of the Ti : Ca with iso mol% up to a *ca.* 97% Ti for iso 90%-L. The FT-IR spectra of these samples reveal distinctive carboxylate and metal vibration bands intrinsic to iso-100% that are also present in iso-L samples due to the very low iso mol% (ESI Section S6†). This suggests that the iso 100% phase is formed at the expense of the MUV-10 phase in iso-L for increasing iso mol%.

We used the excess of Ti obtained by EDX analysis to calculate the fraction of the iso 100% phase formed along with the iso-L series, which increases progressively up to mol 90% of iso where the MUV-10 phase has almost completely disappeared (Fig. 5a). Next, we analyzed the TGA decomposition profiles and ^{1}H-NMR spectra using a model that accounted for the coexistence of MUV-10 and iso 100% phases (ESI Section S6†). The maximum incorporation of defects into iso-L (Fig. 5b) is similar to the iso-H (Table S30†). However, our results reveal that these are not the ideal conditions to promote the formation of pure MUV-10 defective phases.

Compared to iso, total replacement of btc by benzo did not produce any solid. As a result, analysis of benzo-L is much simpler (ESI Section S7†). Roughly, defect promotion in benzo%-L behaves quite similarly to the H region, with slightly higher values. PXRD, FT-IR and EDX/ICP confirm the formation of crystalline, chemically pure defective MUV-10 phases. Just like for the H region, TGA-NMR analysis reveals minimum

changes in the incorporation of benzo into the framework for similar levels of benzo mol% added (Fig. 5b).

## Effect of modulation on the properties of MUV-10 defective phases

In order to understand the effect of modulation on the properties of the resulting MUV-10 phases, we opted to analyse changes in the size and morphology of the crystals together with variations in gas uptake. Changes in the former are generally ascribed to the coordinative interaction of modulators for capped crystal growth whereas the porosity changes are more likely linked to the generation of defective phases by incorporation of the modulator into the framework.

Accordingly, we initially assessed that iso-H and benzo-H modulation has a strong influence on crystal size and morphology compared to pristine MUV-10. See ESI Section S8.1† for individual sample images and histograms of each data set. Iso modulation provokes the loss of octahedral morphology for the formation of rounded nanoparticles (<650 nm) already visible for 20% of the modulator (Fig. 6b). We observe a progressive decrease in crystal size with iso mol% that reaches a minimum of *ca.* 114 ± 29 nm for iso 83%, (Fig. 6f). The effect of benzo is completely different. Modulation resulted in well-defined microcrystals transitioning from octahedral to dodecahedral phases prior to the formation of rounded nano-particles similar to iso-H samples (Fig. 6c–e). The particle size increases upon addition of benzo up to a maximum of 3290 ± 36 nm for benzo 67% and decreases onwards down to 288 ± 39 nm for benzo 98% (Fig. 6f). This suggests a competing influence of the btc : benzo ratio. For small molar percentages, benzo seems to behave mainly as a pH modulator: it facilitates slower deprotonation for longer nucleation times and subsequent growth of larger crystals with a minimum level of incorporation in the framework (Fig. 4c).[11] In turn, higher concentrations maximize coordination competition and are more effective in capping crystal growth thus yielding smaller particles. We hypothesize that the comparatively smaller sizes obtained by iso modulation are an indicator of the higher coordination effectiveness of this dicarboxylic acid, for better crystal growth capping and far superior levels of incorporation of the modulator to the framework. Altogether, our experimental results suggest that iso and benzo behave as defect-promoting capping modulators at high concentrations but iso is a more efficient defect promoter. The effect of modulation on the thermal stability of the solids is small but consistent with comparatively lower decomposition temperatures for the samples featuring higher defectivity for the benzo and iso series, respectively (Fig. S45†). To confirm that defect promotion did not compromise the stability of MUV-10 we dispersed the samples in water at pH 2, 7 and 12 during 24 hours (Section S8.2 and S9.2†). The PXRD patterns of iso-H, benzo-H and benzo-L series show minimum changes to the crystallinity of the framework in all cases. In turn, iso-L samples show reduced stability in acidic and basic media that becomes more abrupt for increasing concentrations of the modulator from 25%. However, the formation of the amorphous iso 100% phase
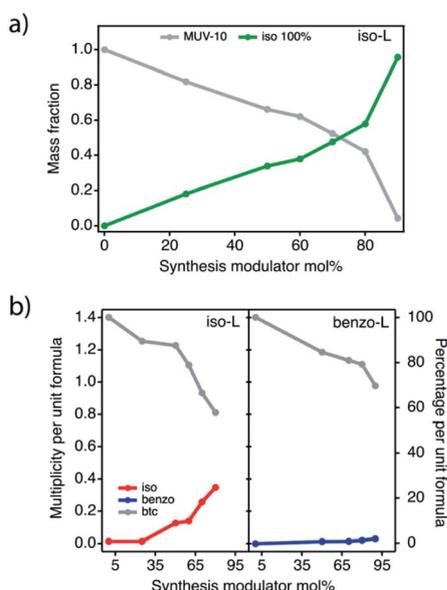


**Fig. 5** (a) Variation of the relative fraction of MUV-10 and iso-100% phases for increasing concentrations of isophthalic acid as estimated from a combination of EDX and TG analysis. (b) Comparison of the amount of btc, isophthalic and benzoic acid in the framework in the L regions for increasing concentrations of the modulator.
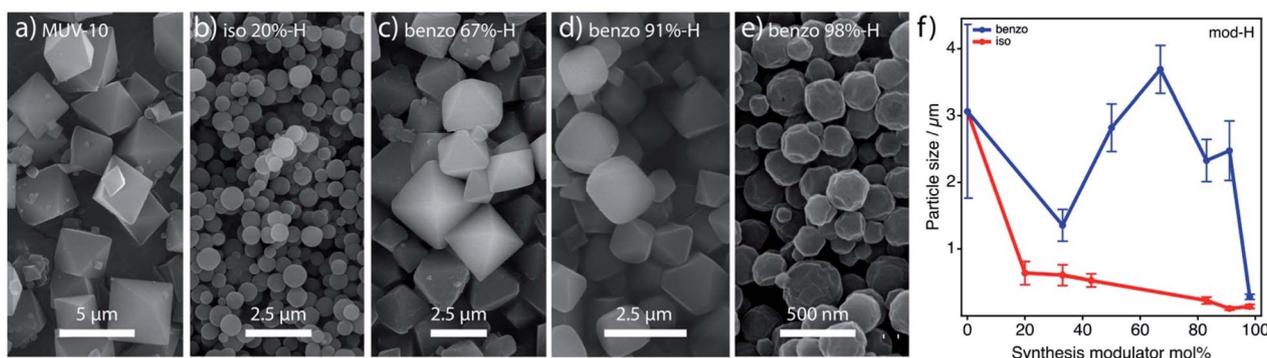
**Fig. 6** SEM pictures comparing the changes in size and morphology of (a) pristine MUV-10, (b) iso 20%-H and benzo-H: (c) 67%, (d) 91% and (e) 98%. (f) Evolution of the particle size as a function of the concentration of the modulator in the H region as estimated from the digital analysis of the SEM images. Error bars stand for the calculated standard deviation.

under these conditions impedes ascribing this effect exclusively to the increased defectivity. We also observe an impact on the wettability of the solids with the promotion of defects (ESI Section S8.3†). Compared to the pristine material, water dispersion is favoured for the most defective iso and benzo samples while their dispersibility in dichloromethane decreases as a consequence of their increased hydrophilicity.

We next evaluated the effect of modulation by comparison of the $N_2$ adsorption isotherms at 77 K of pristine MUV-10 with iso-H and benzo-H samples (see ESI Section S8.4†). MUV-10 displays a type-I isotherm characteristic of microporous materials with a narrow pore size distribution (PSD) centred at 1.0 nm and an experimental surface area of approximately 1000 $m^2$ $g^{-1}$.[24] The nitrogen uptake of iso-H samples does not follow a progressive increase with the modulator mol% added to the synthesis and it shows two different regimes (Fig. 7a, Table S38†). Compared to iso-H for addition below 43%, which leads to a small reduction in the surface area close to 10%, we observe an increase in the gas uptake in the microporous region for iso addition above 43%, which results in an increase in the BET surface areas of close to 20% for a maximum of 1252 $m^2$ $g^{-1}$ for iso 91%. These trends are consistent with the changes in

defectivity in terms of iso incorporation in the framework, as determined by NMR and TGA analysis (Fig. 4c and d). We also observe a tail above $P/P_0$ 0.9 indicative of intergrain mesoporosity above iso 83%. Additionally, the isotherms have moderate gas uptake above the microporous region, characteristic of type II isotherms. This is more clearly seen in the PSD of iso 98% (Fig. 7b), which shows the onset of mesopores likely due to the irregular packing of the smallest nanoparticles of the series. An increase in total pore volume (related to mesoporosity) is observed in relation with iso incorporation and defectivity up to iso 98%, which has a total pore volume similar to that of iso 91% (ca. 0.61 $cm^3$ $g^{-1}$), 1.5 times the pristine MUV-10 pore volume. Benzo modulation has a minimum impact on the surface area of benzo-H materials denoted by changes within the experimental error for all the intervals of explored concentrations (Fig. 7c, Table S39†). This is significantly different from the effect of monocarboxylic modulators reported for UiO-66, which promotes a marked introduction of defects/missing ligands for a systematic increase of the gas uptake with the concentration of the modulator.[26] It is worth noting that benzo 98%-H shows a hysteresis loop at $0.4 < P/P_0 < 0.8$ more characteristic of a type-IV mesoporous material. Our
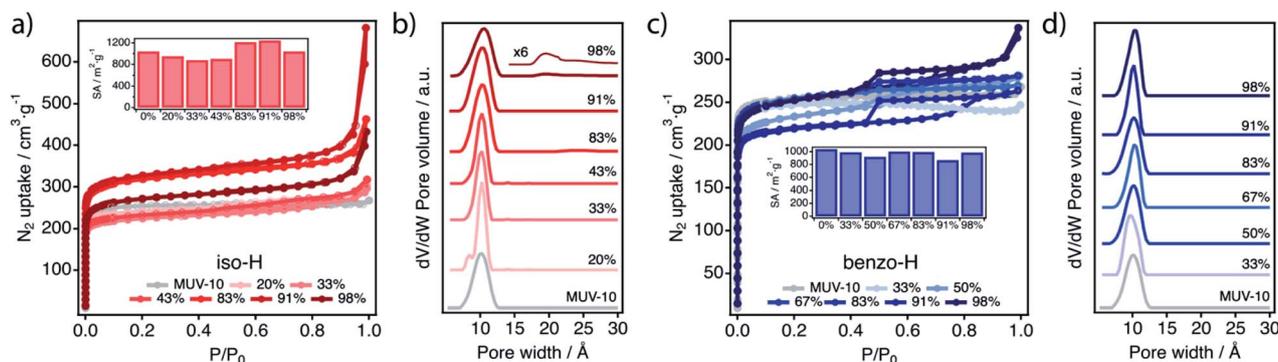


**Fig. 7** $N_2$ adsorption (filled symbol) and desorption (empty symbol) isotherms at 77 K of the series (a) iso-H and (c) benzo-H showing the progressive changes in the uptake profile and surface area with the concentration of the modulator used. (b and d) Changes in the pore size distributions (PSDs) for both sets as calculated by using nonlinear solid density functional theory (NLDFT) by assuming the QSDT cylindrical pore oxide surface model.

results suggest that the higher the defectivity the stronger the impact on the porosity of the material. However, the comparison of the PSD plots for iso-H samples at high modulator concentrations does not show clear differences that might be ascribed to the generation of bigger cavities as a result of the removal of btc units (Fig. 7b). To rationalize this behaviour, we used the structure of defect-free MUV-10 as a starting model to calculate the theoretical PSD of a simulated structure that accounted for 8% and 44% of missing linker positions. These values account for the minimum and maximum levels of iso incorporation determined experimentally for iso-H 33% and 98%. As shown in Fig. S33,† our simulations for a sampling of 12 configurations confirm that the structure of MUV-10 is not ideal to generate significantly bigger cavities by replacement of the organic connector with iso. Although we do not observe significant shifts in the pore size distribution, the increase in the pore volumes is possibly due to both the incorporation of the modulator and the formation of defects for iso-H.

Regarding the L region, the behaviour of the benzo series is quite similar to that of benzo-H samples in terms of crystal size, morphology of the material and porosity changes (ESI Section 9). In the case of iso-L, these properties are dominated by the progressive formation of a bigger fraction of the iso 100% phase at higher concentrations of the modulator. This amorphous solid is composed of Ti and iso precipitates as agglomerates of nanoparticles of <20 nm in size (Fig. S34†). Its formation can be detected even in iso 25%-L as tiny, ill-defined particles decorating the surface of MUV-10 crystals. These particles become more abundant for increasing benzo mol% and as a result, the morphology of the MOF crystals becomes poorly defined. This trend continues up to iso 90%-L for which the MUV-10 phase practically disappeared (Fig. S34†). The iso 100% phase shows a type-IV $N_2$ uptake with a small hysteresis loop $0.4 < P/P_0 < 0.9$ that corresponds to a complex combination of mesopores of different size and shape according to the PSD (Fig. 8, Table S42†). The formation of this phase shows a clear influence on the porosity of iso-L samples that show an increasing predominance of the mesoporous loop for higher modulator

concentrations and a decrease in the gas uptake at the microporous region that is reflected in the PSD. This is particularly abrupt and accompanied by a loss of microporosity for iso-80%-L and onwards. From this point, the relative fraction of the iso-100%-phase prevails over MUV-10 and thus imposes a major change in the properties of the resulting hybrid. The adsorption isotherms and PSDs show relationships with the progressive increase of modulator mol% and the formation of the iso 100% phase. Isotherms do not correspond simply to an overlap of the behaviours of the MUV-10 and iso 100% phases but to an overall porosity that exceeds the sum of the components. As denoted by the complex overlap of pore sizes in the mesopore region of the PSD of iso 90%-L (Fig. 8b), this is possibly due to the intertwined growth of both phases into a hybrid material with abundant packing irregularities associated with the nucleation of the nanosized iso 100% phase particles. The increase in the micropore volume and the decrease in the micropore volume are related to iso incorporation, the mole percent of defects induced in the MUV-10 structure, and the mass fraction of the iso 100% phase, reaching total pore volumes 2 times bigger than that of pristine MUV-10 (Section S.9.3). Although in this work we were mainly interested in rationalising the synthetic conditions that favour defect promotion in titanium frameworks, the drastic changes in porosity triggered by the simultaneous nucleation of MUV-10 and the modulator phase might also be useful in tuning the properties of the hybrid materials prepared under linker deficient conditions. In this direction, we have preliminarily analysed the effect of the incorporation of benzo and iso into the framework on the electronic structure of the solid by using DFT with the HSE06 hybrid functional.[24,31,32] Our results suggest a detrimental effect on the potential photocatalytic activity of the material upon defect incorporation for an increase in the band gap near 0.4 eV (Section S10, Fig. S46†).

## Conclusions

The use of defect chemistry as a synthetic tool for targeted creation of missing linkers must be facilitated by the establishment of clear synthesis-to-structure correlations in defective phases. In this regard, defect engineering should be generalized to a broader range of inorganic nodes beyond UiO-type $Zr_6O_8$ clusters to exploit the rich chemical and structural versatility offered by MOFs. We demonstrate how the promotion of defects in titanium–organic frameworks based on benzene-1,3,5-tricarboxylic linkers can be facilitated by the use of a dicarboxylic modulator. Compared to the poor efficiency of monocarboxylic benzoic acid, isophthalic acid is adequate to favour the promotion of up to 40% of missing linkers in the structure of MUV-10. This difference originates from the ability of the latter to minimize the structural distortion in the defective phase and the higher enthalpy gain associated with the replacement of btc units in the framework. We believe our integrative approach, which combines comprehensive synthesis and characterization with rationalization of the experimental results with computational methods, constitutes a valuable direction to accelerate the creation of targeted defects in MOFs. Even further, our results open the door for the engineering of
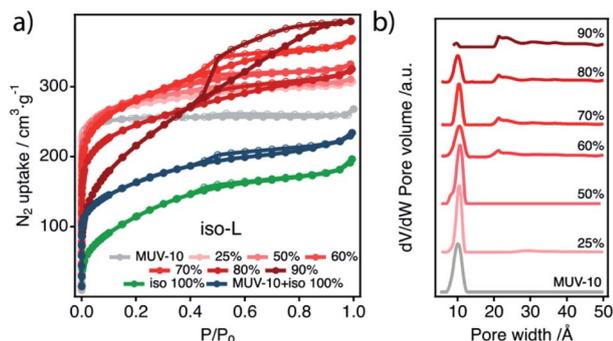


**Fig. 8** (a) $N_2$ adsorption (filled) and desorption (empty symbols) isotherms at 77 K of the iso-L samples, the iso 100% phase and a physical mixture of MUV-10 and the iso 100% phase (50% by weight). (b) PSD of the iso-L series showing the onset of mesoporosity for increasing concentrations of the modulator as calculated with NLDFT by using the QSDT cylindrical pore oxide surface model.

defects in this and other Ti-MOFs, which might be an excellent alternative to fine-tuning the photocatalytic activity of this family of porous materials for controlled sensitization and enhanced performance.

## Conflicts of interest

There are no conflicts to declare.

## Acknowledgements

## References

1 S. Dissegna, P. Vervoorts, C. L. Hobday, T. Düren, D. Daisenberger, A. J. Smith, R. A. Fischer and G. Kieslich, *J. Am. Chem. Soc.*, 2018, **140**, 11581–11584.

2 L. M. R. Albelo, E. L. Maya, S. Hamad, A. R. Ruiz-Salvador, S. Calero and J. A. R. Navarro, *Nat. Commun.*, 2017, **8**, 14457–14467.

3 R. Wei, C. A. Gaggioli, G. Li, T. Islamoglu, Z. Zhang, P. Yu, O. K. Farha, C. J. Cramer, L. Gagliardi, D. Yang and B. C. Gates, *Chem. Mater.*, 2019, **31**, 1655–1663.

4 X. Feng, J. Hajek, H. S. Jena, G. Wang, S. K. P. Veerapandian, R. Morent, N. D. Geyter, K. Leyssens, A. E. J. Hoffman, V. Meynen, C. Marquez, D. E. D. Vos, V. V. Speybroeck, K. Leus and P. V. D. Voort, *J. Am. Chem. Soc.*, 2020, **142**, 3174–3183.

5 A. E. Baumann, X. Han, M. M. Butala and V. S. Thoi, *J. Am. Chem. Soc.*, 2019, **141**, 17891–17899.

6 H.-L. Jiang, X. Ma, L. Wang and Q. Zhang, *Angew. Chem., Int. Ed.*, 2019, **58**, 12175–12181.

7 S. Dissegna, K. Epp, W. R. Heinz, G. Kieslich and R. A. Fischer, *Adv. Mater.*, 2018, **10**, 1704501–1704524.

8 J. Koo, I.-C. Hwang, X. Yu, S. Saha, Y. Kim and K. Kim, *Chem. Sci.*, 2017, **8**, 6799–6803.

9 W. Liang, L. Li, J. Hou, N. D. Shepherd, T. D. Bennett, D. D'Alessandro and V. Chen, *Chem. Sci.*, 2018, **9**, 3508–3516.

10 R. S. Forgan, *Chem. Sci.*, 2020, **11**, 4546–4562.

11 C. R. Marshall, S. A. Staudhammer and C. K. Brozek, *Chem. Sci.*, 2019, **10**, 9396–9408.

12 H. Guo, Y. Zhu, S. Wang, S. Su, L. Zhou and H. Zhang, *Chem. Mater.*, 2012, **24**, 444–450.

13 F. Vermoortele, B. Bueken, G. L. Bars, B. V. de Voorde, M. Vandichel, K. Houthoofd, A. Vimont, M. Daturi, M. Waroquier, V. V. Speybroeck, C. Kirschhock and D. E. D. Vos, *J. Am. Chem. Soc.*, 2013, **135**, 11465–11468.

14 M. Taddei, *Coord. Chem. Rev.*, 2017, **343**, 1–24.

15 M. J. Cliffe, W. Wan, X. Zou, P. A. Chater, A. K. Kleppe, M. G. Tucker, H. Wilhelm, N. P. Funnell, F.-X. Coudert and A. L. Goodwin, *Nat. Commun.*, 2014, **5**, 4176–4184.

16 H. Assi, G. Mouchaham, N. Steunou, T. Devic and C. Serre, *Chem. Soc. Rev.*, 2017, **46**, 3431–3452.

17 M. Dan-Hardi, C. Serre, T. Frot, L. Rozes, G. Maurin, C. Sanchez and G. Férey, *J. Am. Chem. Soc.*, 2009, **131**, 10857–10859.

18 B. Bueken, F. Vermoortele, D. E. P. Vanpoucke, H. Reinsch, C. Tsou, P. Valvekens, T. De Baerdemaeker, R. Ameloot, C. E. A. Kirschhock, V. Van Speybroeck, J. M. Mayer and D. De Vos, *Angew. Chem., Int. Ed.*, 2015, **54**, 13912–13917.

19 J. Castells-Gil, N. M. Padial, N. Almora-Barrios, I. da Silva, D. Mateo, J. Albero, H. García and C. Martí-Gastaldo, *Chem. Sci.*, 2019, **10**, 4313–4321.

20 H. L. Nguyen, F. Gándara, H. Furukawa, T. L. H. Doan, K. E. Cordova and O. M. Yaghi, *J. Am. Chem. Soc.*, 2016, **138**, 4330–4333.

21 A. Cadiau, N. Kolobov, S. Srinivasan, M. G. Goesten, H. Haspel, A. V. Bavykina, M. R. Tchalala, P. Maity, A. Goryachev, A. S. Poryvaev, M. Eddaoudi, M. V. Fedin, O. F. Mohammed and J. Gascon, *Angew. Chem., Int. Ed.*, 2020, **59**, 13468–13472.

22 J. Cao, W. Ma, K. Lyu, L. Zhuang, H. Cong and H. Deng, *Chem. Sci.*, 2020, **11**, 3978–3985.

23 S. Yuan, J.-S. Qin, H.-Q. Xu, J. Su, D. Rossi, Y. Chen, L. Zhang, C. Lollar, Q. Wang, H.-L. Jiang, D. H. Son, H. Xu, Z. Huang, X. Zou and H.-C. Zhou, *ACS Cent. Sci.*, 2017, **4**, 105–111.

24 J. Castells-Gil, N. M. Padial, N. Almora-Barrios, J. Albero, A. R. Ruiz-Salvador, J. González-Platas, H. García and C. Martí-Gastaldo, *Angew. Chem., Int. Ed.*, 2018, **57**, 8453–8457.

25 N. M. Padial, B. Lerma-Berlanga, N. Almora-Barrios, J. Castells-Gil, I. da Silva, M. de la Mata, S. I. Molina, J. Hernández-Saz, A. E. Platero-Prats, S. Tatay and C. Martí-Gastaldo, *J. Am. Chem. Soc.*, 2020, **142**(14), 6638–6648.

26 G. C. Shearer, S. Chavan, S. Bordiga, S. Svelle, U. Olsbye and K. P. Lillerud, *Chem. Mater.*, 2016, **28**, 3749–3761.

27 G. Cai and H.-L. Jiang, *Angew. Chem., Int. Ed.*, 2017, **56**, 563–567.

28 R. Röder, T. Preiß, P. Hirschle, B. Steinborn, A. Zimpel, M. Höhn, J. O. Rädler, T. Bein, E. Wagner, S. Wuttke and U. Lächelt, *J. Am. Chem. Soc.*, 2017, **139**, 2359–2368.

29 L. Valenzano, B. Civalleri, S. Chavan, S. Bordiga, M. H. Nilsen, S. Jakobsen, K. P. Lillerud and C. Lamberti, *Chem. Mater.*, 2011, **23**, 1700–1718.

30 I. A. Lázaro, *Eur. J. Inorg. Chem.*, 2020, **2020**, 4284–4294.

31 N. M. Padial, J. Castells-Gil, N. Almora-Barrios, M. Romero-Angel, I. da Silva, M. Barawi, A. García-Sánchez, V. A. d. l. P. O'Shea and C. Martí-Gastaldo, *J. Am. Chem. Soc.*, 2019, **141**, 13124–13133.

32 K. L. Svane, J. K. Bristow, J. D. Gale and A. Walsh, *J. Mater. Chem. A*, 2018, **6**, 8507–8513.